Thermal Stability of Precursors for Atomic Layer Deposition of TiO_2, ZrO_2, and HfO_2: An Ab Initio Study of α-Hydrogen Abstraction in Bis-cyclopentadienyl Dimethyl Complexes

Aleksandra Zydor* and Simon D. Elliott†

Tyndall National Institute, University College Cork, Lee Maltings, Cork, Ireland

Received: July 29, 2009; Revised Manuscript Received: October 19, 2009

Thin film dielectrics based on hafnium and zirconium oxides are being introduced to increase the permittivity of insulating layers in nanoelectronic transistor and memory devices. Atomic layer deposition (ALD) is the process of choice for fabricating these films, and the success of this method depends crucially on the chemical properties of the precursor molecules. Designing new precursors requires molecular engineering and chemical tailoring to obtain specific physical properties and performance capabilities. A successful ALD precursor should be volatile, stable in the gas-phase, but reactive on the substrate and growing surface, leading to inert byproduct. This study is concerned with the thermal stability in the gas phase of Ti, Zr, and Hf precursors that contain cyclopentadienyl ($Cp = C_5H_{5-x}R_x$) ligands. We use density functional theory (DFT) to probe the non-ALD decomposition pathway and find a mechanism via intramolecular α-H transfer that produces an alkylidene complex. The analysis shows that thermal stabilities of complexes of the type $MCp_2(CH_3)_2$ increase down group 4 (M = Ti, Zr, and Hf) due to an increase in the HOMO−LUMO band gap of the reactants, which itself increases with the electrophilicity of the metal. Precursor decomposition via this pathway in the gas phase can therefore be avoided by replacing the α-H donor or acceptor ligands or by increasing the electrophilicity of the metal. This illustrates how the ALD process window can be widened by rational molecular design based on mechanistic understanding.

I. Introduction

Thin films based on zirconia (ZrO_2) or hafnia (HfO_2) are being used as high-permittivity dielectrics in the latest generation of transistors and show promise as insulating layers in memories and high-value capacitors.[1] This has in part been enabled by the development of atomic layer deposition (ALD) processes for these materials, delivering films of high purity and uniformity with sub-nanometer thickness control.[2] The ALD process depends intimately on the chemistry of the precursor molecules, so considerable attention is now being paid to the design, synthesis, and properties of organometallic compounds of Zr and Hf.

ALD is a special type of chemical vapor deposition (CVD) in which precursors are admitted separately into the reactor.[2] Ideal ALD is achieved if the reaction of the precursor with the surface is self-limiting, finishing once the surface is saturated with precursor fragments (e.g., ligands or hydroxyl groups). Sufficient precursor exposure will then lead to uniform film growth, even coating complex three-dimensional substrates. To achieve ALD's unique characteristic, the precursor must have specific properties. It should be volatile and vaporize rapidly at the reproducible rate, conditions that are usually met for liquid precursors but not for solids. For self-terminating surface reactions it should not self-react, but it should be reactive on the substrate and growing surface. However, many precursor molecules undergo intra- or intermolecular reactions, either in the gas phase or on the surface, that do not self-limit and are termed decomposition reactions. In general, such non-ALD decomposition is thermally activated, and so can also be significant when the precursor is heated to volatilize it or when it enters the heated chamber of the ALD reactor. Non-ALD decomposition can lead to the waste of precursor chemicals, uncontrolled film growth, impure films, poor thickness control, and uneven coating in two and three dimensions. For example, Zr and Hf amide precursors show deleterious decomposition as the reactor temperature is increased. As-deposited hafnium oxide films showed nonuniformity that increased from 1 to 5% of the film thickness as the deposition temperature was raised, indicating a contribution from non-ALD decomposition reactions. For zirconium oxide, similar roughness was already observed at much lower deposition temperatures.[3]

Recently, a new family of cyclopentadienyl precursors of Zr and Hf has been introduced,[4] some of which show enhanced thermal stability and are more suitable for high-temperature growth. The stability of the family of cyclopentadienyl precursors has been investigated in static thermogravimetric experiments, revealing a significant difference between the stability of Zr and Hf compounds: the involatile residues for $Hf(MeCp)_2Me_2$ and $Zr(MeCp)_2(OMe)Me$ are very low (<2%), indicating that no significant decomposition occurs as the precursors are volatilized.[5] In contrast, the very high residue (>50%) observed for $Zr(MeCp)_2Me_2$ shows that decomposition occurs under relatively mild conditions (∼200 °C). $Zr(MeCp)_2Me_2$ decomposes violently after 4 h at 160 °C.

Currently, little is known about these differences in thermal stability and about the underlying mechanism of decomposition of ALD precursor molecules. However, to design new ALD precursors and develop and optimize an ALD process for the deposition of new materials requires knowledge of the reaction mechanism. Most of the studies on ALD modeling have been dedicated to ALD mechanisms[6] and the reactions of precursors with the surface.[7,8] The presence of thermal decomposition

* To whom correspondence should be addressed. E-mail: aleksandra.zydor@tyndall.ie.

† E-mail: simon.elliott@tyndall.ie.

10.1021/jp9072608 © 2010 American Chemical Society
Published on Web 01/07/2010

means that we also need to understand the mechanism of precursor reactions that happen in the gas phase. Therefore, the aim of our studies is to investigate possible decomposition reaction pathways and to explain the observed differences in thermal stability. The precursor complexes that are the subject of this study are denoted ML_2Me_2, where M is a group 4 metal M = Ti, Zr, or Hf and the ligands are L = Cp, MeCp, OMe, and Me (Me = CH_3).

The molecules that we study here are new to the ALD research area but have been widely studied in organometallic and organic synthesis. A derivative of the Ti complex functions as a Ziegler−Natta polymerization catalyst.[9] Tebbe et al.[10] discovered that a complex derived from titanocene dichloride and trimethylaluminium olefinates carbonyl compounds,[11,12] such as ketones, aldehyde, and amides. For esters and thioesters it is more efficient to use dimethyl titanocene (the Petasis reagent),[11] which undergoes thermal elimination of CH_4 from the position α to the metal, to afford a titanium alkylidene complex ($Cp_2Ti{=}CH_2$), also known as a Schrock carbene.[13,14] Alkylidenes can generally be obtained by the α-deprotonation of di- or polyalkyl complexes of coordinatively saturated early transition metals in high oxidation states (d^0).[15]

It is known that the reactivity of tetraalkyl complexes of transition metals strongly depends on steric effects between the alkyl ligands and on the identity of the metal itself,[13,16] affecting both the mechanism and the energetics of the decomposition reaction. Two mechanisms were studied in the case of tetramethyl complexes of Ti, Zr, and Hf: intramolecular and intermolecular α-H abstraction.[17] Schrock and others have postulated that when the alkyl group is small, e.g., methyl, the first step is bimolecular α-hydrogen abstraction, which is rate-determining.[13,18−21] The calculated activation enthalpies according to the bimolecular mechanism are in the order $ZrMe_4$ (64.9 kJ/mol) < $HfMe_4$ (82.8 kJ/mol) ∼ $TiMe_4$ (83.7 kJ/mol), which is in agreement with measurements.[16,17,22]

When the alkyl group becomes bulkier, the bimolecular mechanism becomes unfavorable because of steric reasons and the unimolecular mechanism becomes favored instead. In the case of complexes with bulkier alkyl ligands, theory and experiment show the stability increasing in the order $TiNp_4$ < $ZrNp_4$ < $HfNp_4$ (Np = neopentyl C_5H_{11}), which is consistent with unimolecular decomposition.[17,23] Indeed, unimolecular α-H abstraction is found to proceed readily in group 4 organometallics where there is significant crowding and a suitable acceptor ligand, with first-order reaction kinetics indicative of a rate-determining step, where C−H bonds are made and broken in a cyclic reaction path.[17,24] Consistent with this, CH_4 was observed as a product of the decomposition of $TiCp_2Me_2$, $ZrCp_2Me_2$, and $HfCp_2Me_2$, and it was shown that dissociation of the M−Me bond or abstraction of H from a methyl group is the rate-determining step.[25] The thermal stability of these compounds is found to increase down group 4, which suggests an electronic effect at the metal center. The question of steric versus electronic effects has also been discussed for niobium and tantalum alkylidenes.[13] It is suggested that any change in the ligands that increases the electrophilicity of the metal should increase the rate of α-H abstraction and elimination of CH_4. Looking here at group 4, the chemistry of Zr and Hf compounds is very similar to one another. In particular, the ground-state properties of ZrO_2 and HfO_2, such as their structure and vibrational frequencies, are very similar.[26] By contrast, the difference in excited-state properties is much greater; e.g., the adiabatic electron affinity of HfO_2 was determined to be 2.14 ± 0.03 eV, and that of ZrO_2 was determined to be 1.64 ± 0.03 eV, indicating that HfO_2 is more ionic than ZrO_2.[26]

Therefore, in the ML_2Me_2 complexes that we study here, bulky ligands (such as L = Cp) may favor unimolecular α-H transfer between the methyl ligands, and there may be electronic reasons for differences between M = Ti, Zr, and Hf. We propose eq 1 as a possible decomposition pathway:

$$ML_2Me_2 \rightarrow ML_2(CH_2) + CH_4 \quad (1)$$

As outlined above, there is much evidence for α-hydrogen abstraction during the decomposition of transition metal complexes. The aim of our work is to investigate and understand the mechanism of α-hydrogen abstraction in the case of MCp_2Me_2 complexes for M = Ti, Zr, and Hf, which is possibly the first step in their decomposition. We use density functional theory (DFT) to calculate the electronic and molecular structure and characterize this decomposition pathway (precursors, transition states (TSs), and products; activation energy E_a and reaction energy ΔE). To find out what role is played by the nonreacting ligands (spectator ligands) L, the calculations were also performed for L = MeCp, Me, and OMe in the complexes ZrL_2Me_2. In the case of $Zr(MeCp)_2Me_2$ we briefly test the competing reaction of β-hydrogen abstraction. For a series of choices of metal M = Ti, Zr, and Hf and ligand L = Cp, MeCp, Me, and OMe, we use DFT vibrational analyses to confirm the nature of the stationary points and to obtain entropy and free energy changes.

As illustrated by the catalytic activity mentioned above, the carbene product is highly reactive, so it is likely that further unimolecular or bimolecular reactions follow eq 1. We do not attempt to calculate this wide range of subsequent reactions. However, we include a brief study of β-H abstraction as a competing first-step (eq 2) or second-step reaction (eq 3) of decomposition process, as was suggested for related molecule $TiCp^*_2Me_2$ ($Cp^* = C_5Me_5$).[20]

II. Theoretical Methods

The precursor molecules and their ALD reaction products were modeled as isolated molecules in vacuum. The ground-state electronic wave function of each molecule was calculated self-consistently within Kohn−Sham DFT using the TURBOMOLE suite of quantum chemical programs.[27] All species were closed shell. Unconstrained optimization of the molecular geometry was carried out on the DFT potential energy hypersurface. Vibrational analysis was performed for each considered structure in order to characterize the nature of the stationary point. A stationary point found by a geometry optimization is a minimum (local or global following its stability) when all the vibrational frequencies are real. In contrast, it is a TS linking two minima when there is one imaginary frequency. A good trade-off between accuracy and computational cost was obtained by using the B-P86 functional, the RI approximation,[28−30] and the atom-centered TZVP(P) basis set[31] with effective core potentials of 28 electrons on Zr and of 60 electrons on Hf.[32]

III. Results

III.1. Decomposition Pathway. The computed reaction coordinate for eq 1 is primarily the transfer of H from one methyl group to the other, producing CH_4 which dissociates from the complex, leaving methylene bound to the metal center in $ML_2(CH_2)$ (Figure 1). H-transfer is coupled with the slight

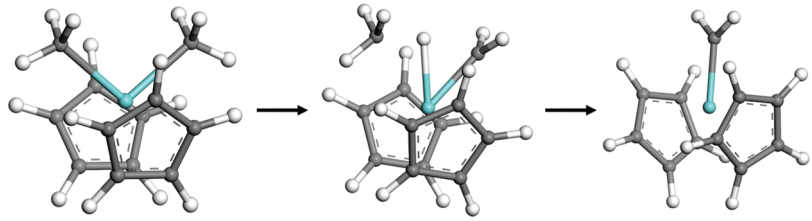

Figure 1. Ball and stick representations of computed structures of precursor (reactant), TS, and product along the decomposition pathway (eq 1) for L = Cp and M = Zr: white = hydrogen; gray = carbon; blue = Zr.

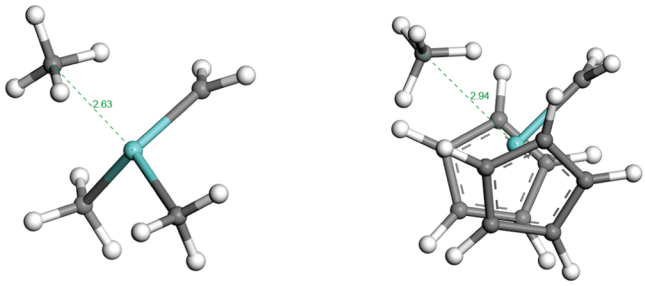

Figure 2. Ball and stick representations of the computed structure of the intermediate occurring during the decomposition pathway (eq 1) for L = Me, Cp and M = Zr: white = hydrogen; gray = carbon: blue = Zr. The depth of the minimum of the intermediates is reflected in the M−C(CH_4) distances: 2.94 and 2.63 Å for L = Cp and Me, respectively.

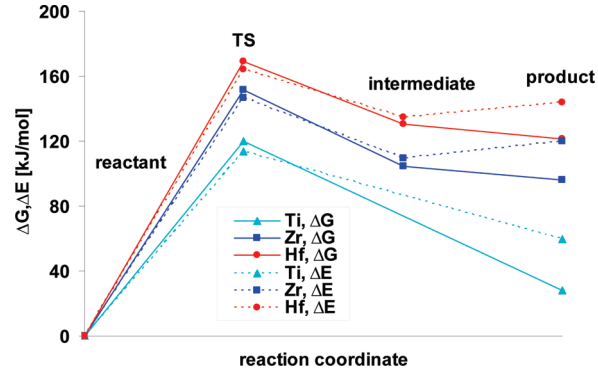

Figure 3. Computed energetics along the decomposition pathway from the data in Table 1. Lines are to guide the eye.

TABLE 1: Energetics along the Decomposition Pathway Equation 1 Computed Using DFT[a]

		$TiCp_2Me_2$	$ZrCp_2Me_2$	$HfCp_2Me_2$
TS	E_a (kJ/mol)	114	147	164
	S_a (kJ/mol·K)	−0.020	−0.016	−0.016
	G_a (kJ/mol)	120	151	169
intermediate	ΔE (kJ/mol)		109	135
	ΔS (kJ/(mol·K))		0.016	0.015
	ΔG (kJ/mol)		104	130
product	ΔE (kJ/mol)	60	120	145
	ΔS (kJ/(mol·K))	0.106	0.080	0.077
	ΔG (kJ/mol)	28	96	121

[a] Positive values indicate an energetic cost relative to the reactants. The Gibbs free energy is obtained from $\Delta G = \Delta H - T\cdot\Delta S$ at $T = 298$ K. Illustrated in Figure 3.

contraction of the C(CH_4)−M−C(CH_2) angle, where in our notation C(CH_4) represents a carbon atom in a leaving methyl group and C(CH_2) is a carbon atom of the remaining methyl group. At the TS, the four atoms involved in the reaction are coplanar, namely, C(CH_4), C(CH_2), H, and M.

The computed energetics of eq 1 for L = Cp are presented in Table 1 and Figure 3. The activation energy and overall endothermicity become greater down the group, with the Ti complex most likely to decompose, the Zr complex substantially more stable, and the Hf complex slightly more stable again. The decomposition reaction leads to a carbene product of higher energy than compared to the reactant, and this carbene is in turn likely to be highly reactive. The stability of the carbene product decreases down the group. The reasons for these differences are explored below. The entropic contribution is slightly less at the TS but increases substantially as the second product molecule is formed, lowering ΔG for the overall reaction by over 20 kJ/mol at 298 K.

In the cases of M = Zr and Hf, the DFT energies show a slight minimum in the dissociation channel (Figure 2) consisting of weakly bound CH_4, which opens up the possibility of the reverse reaction occurring. However, this minimum disappears when corrected for entropy at $T > 0$.

For the corresponding decomposition reaction of $Zr(MeCp)_2(Me)(OMe)$ to $Zr(MeCp)_2(CH_2)$ and MeOH the computed reaction energy is $\Delta E = 299$ kJ/mol, but we were unable to find a TS which leads to these products. However, we found a minimum on the dissociation channel similar to the intermediates presented in Figure 2. The energy cost for the formation of this intermediate compared to the reactant is $\Delta E = 217$ kJ/mol.

III.2. Effect of the Metal Cation. To understand the different decomposition behavior of M = Ti, Zr, and Hf, we have analyzed their atomic and electronic structure along the reaction pathway for L = Cp. Table 2 lists the most important structural parameters.

The primary factor is the size of the cation: M−C distances are consistently 0.10−0.15 Å shorter for M = Ti than for the other M, while those for Zr and Hf are generally identical to within 0.01 Å. However in all cases, the M−C(CH_2) distance decreases by 0.2 Å as M−C(CH_2) is transformed into M=C(CH_2), and most of this decrease has already occurred when the TS is reached. The angle that the methyl ligands subtend at the metal center in the reactant complex is 94° for M = Ti and 98−100° for M = Zr and Hf. This narrows to a more consistent 81−83° at the TS.

Ti−Cp distances remain roughly constant throughout the reaction, but the Cp ligands have space to move apart in the product, as evidenced by the wider $Cp_{cent.}$−Ti−$Cp_{cent.}$ angle. For Zr and Hf, the product complexes show a similar widening of this angle, accompanied here by a 0.05 Å shortening of M−$Cp_{cent.}$.

The electronic structure of the reactants, transition states, and products is analyzed in terms of the HOMO (highest occupied molecular orbital), LUMO (lowest unoccupied molecular orbital), and energy gap between these orbitals (Table 3). Since DFT functionals such as B-P86 systematically underestimate the energies of unoccupied orbitals, we consider only the trends across these systems. The HOMO is nearly degenerate with the HOMO-1 in the reactant (because of near-symmetry), and these orbitals are the only occupied ones to show significant M:*d*

TABLE 2: Selected Parameters of the DFT Optimized Structures of MCp_2Me_2 (Reactants), M = Ti, Zr, or Hf, Transition States and Products According to Equation 1[a]

	$TiCp_2Me_2$			$ZrCp_2Me_2$			$HfCp_2Me_2$		
	reactant	TS	product	reactant	TS	product	reactant	TS	product
				Distance (Å)					
$M-C(CH_2)$	2.18	1.98	1.95	2.29	2.09	2.07	2.28	2.09	2.07
$M-C(CH_4)$	2.18	2.46		2.29	2.55		2.28	2.55	
M−H	2.85	1.80		2.851	1.94		2.856	1.94	
$C(CH_4)-H$	1.10	1.41		1.10	1.40		1.10	1.37	
$C(CH_2)-H$	1.10	1.57		1.10	1.66		1.10	1.71	
$M-Cp_{cent.}$	2.10	2.10	2.09	2.26	2.24	2.22	2.26	2.24	2.21
$M-Cp_{cent.}$	2.10	2.08	2.05	2.25	2.24	2.22	2.26	2.24	2.21
				Angle (deg)					
$C(CH_4)-M-C(CH_2)$	94.4	83.2		99.8	81.3		97.8	82.1	
$Cp_{cent.}-M-Cp_{cent.}$	134.9	131.4	143.0	133.5	136.9	144.4	133.2	136.3	143.8

[a] The centroid of the C atoms of Cp is denoted $Cp_{cent.}$. $C(CH_4)$ represents a carbon atom in a leaving methyl group and $C(CH_2)$ represents a carbon atom of the remaining methyl group.

TABLE 3: Analysis of HOMO (Highest Occupied Molecular Orbital) and LUMO (Lowest Unoccupied Orbital) during Decomposition (Energy Level of the HOMO and LUMO (E_h), Energy Gap between HOMO and LUMO (ε_g), Total Charge Density q of Metal Cation [M] from Mulliken Population Analysis)

		reactant	TS	product
$TiCp_2Me_2$	ε_g (kJ/mol)	290	265	129
	LUMO (E_h)	−0.100	−0.064	−0.114
	HOMO (E_h)	−0.211	−0.165	−0.163
	q [Ti]	0.17	−0.02	0.35
$ZrCp_2Me$	ε_g (kJ/mol)	349	288	135
	LUMO (E_h)	−0.078	−0.052	−0.106
	HOMO (E_h)	−0.211	−0.162	−0.157
	q [Zr]	0.56	0.17	0.41
$HfCp_2Me_2$	ε_g (kJ/mol)	373	298	125
	LUMO (E_h)	−0.068	−0.044	−0.104
	HOMO (E_h)	−0.210	−0.158	−0.152
	q [Hf]	0.62	0.25	0.49

character. Plotting these orbitals (Figure 4) reveals that they are three-center σ-bonding between M and the two C_{2v}-symmetric $C(CH_3)$ atoms, but the proportion of M character in Mulliken population analysis is seen to be slightly more for Ti than for Zr and Hf (not quoted here). There is a very small contribution from Cp:π to the HOMO.

The LUMO of the reactant is of predominantly M:d character (not plotted here), and its energy rises down the group Ti, Zr, Hf. Consequently, the energy gap from HOMO to LUMO is strongly dependent on M, increasing down the group from 290 kJ/mol for M = Ti to 373 kJ/mol for M = Hf (Table 3). On the basis of the total charge density from Mulliken population analysis, the positive charge of M also increases down the group (Table 3), consistent with higher ionicity.

C_{2v} symmetry is lifted as H-transfer proceeds. Both HOMO and LUMO shift in energy. In all of the Cp complexes the HOMO becomes destabilized as the reaction proceeds. At the transition state, the energy of the LUMO also rises but then falls in the product.

As the reaction proceeds, the HOMO−LUMO energy gap decreases for all the complexes leading to the products of almost identical HOMO−LUMO gaps (125−135 kJ/mol). In contrast with the reactants, the product complexes show very similar HOMO orbital structures for M = Ti, Zr, and Hf.

At the TS we see the electron density in the HOMO shifting from $C(CH_4)$ to both $C(CH_2)$ and M. The product HOMO is of predominantly $C(CH_2)$:p, and M:d character, and plots of this orbital confirm that it is $M{=}C(CH_2)$ π-bonding (Figure 4). At the TS, calculations show a negligible HOMO population on the transferring H and negligible change in the overall electron density on that H, suggesting the transfer of neutral H. Already at the TS we see the creation of new bonding between the H and $C(CH_4)$ of length 1.399 Å. On the basis of this, we propose in Figure 5 the way that HOMO electrons are transferred along the decomposition pathway.

III.3. Effect of the Spectator Ligands. To determine what role is played by the nonreacting ligands (spectator ligands) in the unimolecular decomposition reaction (eq 1), we have considered this reaction pathway for a variety of alternative nonreacting ligands L = Cp, MeCp, Me, and OMe in the complexes ZrL_2Me_2. It has been shown, however, that, in the case of smaller spectator ligands (L = Me), the decomposition reaction in fact proceeds by bimolecular, intermolecular α-hydrogen abstraction because of the release of steric interactions.[17]

The computed energetics of eq 1 for L = Cp, Me, and OMe are presented in Figure 6 and Table 4. We see that the identity of the nonreacting ligand has a strong impact on the decomposition reaction. The activation energy and overall endothermicity become greater when replacing Cp with Me and OMe. The most likely complex to decompose is $ZrCp_2Me_2$, which has the lowest activation energy, while $ZrMe_4$ and then $Zr(OMe)_2Me_2$ seem to be more stable in this decomposition pathway. In all the cases of L = Cp, OMe, and Me the DFT energies show a minimum in the dissociation channel, as was shown already for $ZrCp_2Me_2$. However, in contrast to $ZrCp_2Me_2$, the minimum for L = Me and OMe (Figure 6) is deeper and does not quite disappear when corrected for entropy at $T > 0$, which opens up the possibility of the reverse reaction occurring. The entropic contribution is small at the TS for all the complexes, decreasing for L = MeCp, Cp, and OMe but increasing for L = Me. The entropy increases substantially as the product molecules are formed, lowering ΔG for the overall reaction by 24, 39, 29, and 44 kJ/mol for L = Cp, MeCp, OMe, and Me, respectively, at T = 298 K.

To understand the influence of spectator ligands L = Cp, MeCp, Me, and OMe on different decomposition behaviors of ZrL_2Me_2 complexes, we have analyzed their atomic and electronic structure along the reaction pathway eq 1. Table 5 lists the most important structural parameters.

The effect of the spectator ligands on the reacting ligands is particularly reflected in the $C(CH_4)-Zr-C(CH_2)$ angles. The angle to which the reacting methyl ligands subtend at the metal center in the reactant complex is 107° for $Zr(OMe)_2Me_2$ and due to tetrahedral symmetry is 109° for $ZrMe_4$, while in the Cp

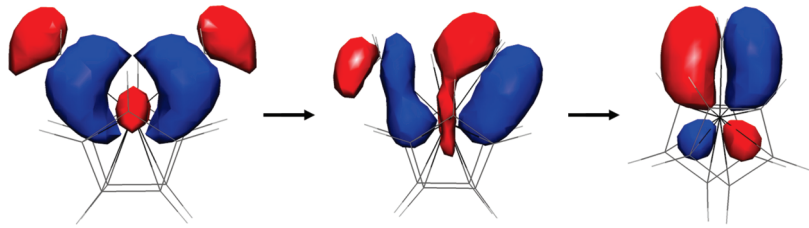

Figure 4. Plotted HOMO orbitals of computed structures of reactant, transition state, and product along decomposition pathway (eq 1) for L = Cp and M = Zr.

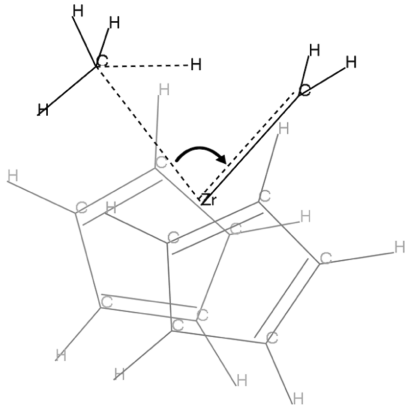

Figure 5. Line representations of computed structure of TS occurring during the decomposition pathway (eq 1) for M = Zr and L = Cp. Bond lengths indicate that a partial $C(CH_4)-H$ bond (dotted line) is formed in the TS. The arrow indicates the observed transfer of HOMO electrons during the decomposition. The spectator ligands are in gray.

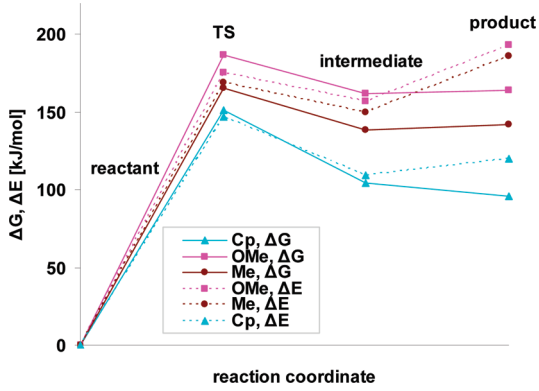

Figure 6. Computed energetics along the decomposition pathway (eq 1) from the data in Table 4. Lines are to guide the eye.

complex it is tightened up to 100°. This narrows to a more consistent 81−86° at the TS for all complexes, although here again we see the steric effect of the Cp ligands, tightening up the $C(CH_4)-Zr-C(CH_2)$ angle by about 5°.

$Zr-C(CH_2)$ distances differ slightly (<0.1 Å) in the reactants. In all cases the $Zr-C(CH_2)$ distance decreases by 0.22−0.24 Å as $Zr-C(CH_2)$ is transformed into $Zr{=}C(CH_2)$, and most of this decrease has already occurred when the TS is reached.

M−L distances of spectator ligands remain roughly constant throughout the reaction. As a result of the decreasing $C(CH_4)-Zr-C(CH_2)$ angle at the TS, the spectator ligands have space to move apart, as evidenced by the wider L−M−L angle. This angle keeps increasing along the decomposition pathway for Cp and OMe but decreases back to 111° in the case of the $ZrMe_4$ complex.

The electronic structure of the HOMO during the decomposition reaction of $ZrMe_4$ and $ZrMe_2(OMe)_2$ is presented in Table 6 in terms of the energy level of the HOMO and LUMO as well as the energy gap between these orbitals. We repeat in the tables here the information on $ZrMe_2Cp_2$ to better explain the effect of spectator ligands in the group of Zr complexes.

Mulliken population analysis along the reaction pathway shows a gradual transfer of HOMO electron density from a three-center σ $C(CH_4)-Zr-C(CH_2)$ bond (in the case of $ZrMe_2(OMe)_2$) and a five-center σ $C_2(Me)-Zr-C_2(Me)$ bond (in case of $ZrMe_4$) to a two-center π $Zr{=}C(CH_2)$ bond, similar to that detailed above for L = Cp. The product has two occupied orbitals localized on $Zr{=}C(CH_2)$, the higher of which is of Zr:*d*−C:*p* π-bonding character similar to all product complexes.

Mulliken population analysis reveals that HOMO and HOMO-1 orbitals show significant M:*d* character. The proportion of M character is seen to be more for the $ZrMe_4$ complex than for $ZrCp_2Me_2$ and $ZrMe_2OMe_2$ complexes. As in all Cp complexes, the LUMO of L = Me and OMe complexes are also of predominantly M:*d* character. As presented in Table 6, the energy gap from HOMO to LUMO is strongly dependent on nonreacting ligands. The influence of Cp ligands is clearly seen here: the energy gap is 62−67 kJ/mol lower compared to L = Me and OMe.

Examining the HOMO and LUMO energies of the reactants reveals two different causes for the greater band gap when Cp is replaced by Me or OMe. In the reactant $ZrMe_4$, four orbitals show Zr−C character. As expected in tetrahedral symmetry, three of them are degenerate in energy and constitute the HOMO. In total, eight electrons are delocalized over both reacting and spectator Me ligands. More delocalization means that the HOMO is much lower in energy than in the Cp and OMe cases, and the band gap is correspondingly higher. In contrast, Cp and OMe spectator ligands have very little contribution to the reactant HOMO in their respective complexes. The L = OMe spectator is seen to drive up the LUMO energy level, again opening the band gap. This destabilization of empty Zr:*d* states is also reflected in the highly ionic character of the Zr center q[Zr] in Table 6), consistent with the nucleophilic ligands L = OMe. Once more, the differences between the complexes with different L are most obvious in the reactants and less marked in the product.

III.4. Possible Reaction of "Spectator" Ligands. In a case of the $Zr(MeCp)_2Me_2$ complex we have also investigated the possibility of decomposition via β-hydrogen abstraction from one methyl group of the MeCp ligand, yielding a tuck-in complex according to eq 2

$$Zr(MeCp)_2Me_2 \rightarrow Zr(MeCp)(C_5H_4CH_2)Me + CH_4 \quad (2)$$

The activation energy is calculated to be E_a = 144 kJ/mol and Gibbs free energy G_a = 156 kJ/mol at T = 298 K, with some variation with rotation of the two MeCp units. This activation energy is comparable with that computed for α-hy-

TABLE 4: Energetics along the Decomposition Pathway (Equation 1) Computed Using DFT[a]

		$ZrCp_2Me_2$	$Zr(MeCp)_2Me_2$	$ZrMe_4$	$Zr(OMe)_2Me_2$
TS	E_a (kJ/mol)	147	150	169	175
	S_a (kJ/(mol·K))	−0.016	−0.008	0.012	−0.038
	G_a (kJ/mol)	151	152	166	187
intermediate	ΔE (kJ/mol)	109	114	150	157
	ΔS (kJ/(mol·K))	0.016	−0.025	0.037	−0.018
	ΔG (kJ/mol)	104	122	139	162
product	ΔE (kJ/mol)	120	121	186	193
	ΔS (kJ/(mol·K))	0.080	0.130	0.147	0.098
	ΔG (kJ/mol)	96	82	142	164

[a] Positive values indicate an energetic cost relative to the reactants. The Gibbs free energy is obtained from $\Delta G = \Delta E - T\cdot\Delta S$ at $T = 298$ K. Illustrated in Figure 6.

TABLE 5: Selected Parameters of the DFT-Optimized Structures of ZrL_2Me_2 (Reactants), L = Cp, Me, OMe, Transition States and Products According to Equation 1[a]

	$ZrCp_2Me_2$			$Zr(OMe)_2Me_2$			$ZrMe_4$		
	reactant	TS	product	reactant	TS	product	reactant	TS	product
symmetry	C_{2v}	C_1	C_{2v}	C_{2v}	C_1	C_s	T_d	C_1	C_s
				Distance (Å)					
$M-C(CH_2)$	2.29	2.09	2.07	2.25	2.06	2.02	2.23	2.04	1.99
$M-C(CH_4)$	2.29	2.55		2.25	2.46		2.23	2.42	
$M-L/Cp_{cent.}$	2.26	2.24	2.22	1.93	1.95	1.94	2.23	2.25	2.23
				Angle (deg)					
$C(CH_4)-M-C(CH_2)$	99.8	81.3		107.1	85		109.5	86.0	
L−M−L	133.5	136.9	144.4	117.3	125.5	128.5	109.5	115.2	110.8

[a] The centroid of the C atoms of Cp is denoted $Cp_{cent.}$. The point symmetry group of each molecule is also given. $C(CH_4)$ represents a carbon atom in a leaving methyl group and $C(CH_2)$ represents a carbon atom of the remaining methyl group.

TABLE 6: Analysis of HOMO (Highest Occupied Molecular Orbital) and LUMO (Lowest Unoccupied Orbital) during Decomposition (Energy Level of the HOMO and LUMO (E_h), Energy Gap between HOMO and LUMO (ε_g), Total Charge Density q of Metal Cation [M] from Mulliken Population Analysis)

		reactant	TS	product
$ZrMe_2Cp_2$	ε_g (kJ/mol)	349	288	135
	LUMO (E_h)	−0.078	−0.052	−0.106
	HOMO (E_h)	−0.211	−0.162	−0.157
	q [Zr]	0.56	0.17	0.41
$ZrMe_4$	ε_g (kJ/mol)	411	285	170
	LUMO (E_h)	−0.070	−0.071	−0.104
	HOMO (E_h)	−0.227	−0.180	−0.169
	q [Zr]	0.89	0.93	0.91
$ZrMe_2OMe_2$	ε_g (kJ/mol)	416	327	147
	LUMO (E_h)	−0.052	−0.040	−0.097
	HOMO (E_h)	−0.210	−0.165	−0.153
	q [Zr]	1.22	0.94	0.97

drogen abstraction. However, in the case of $TiCp^*_2Me_2$, isotope labeling experiments show that this reaction plays a minor part in decomposition (only 2% of the product).[20] Alternatively, the same tuck-in complex $Zr(MeCp)(C_5H_4CH_2)Me$ could be formed by intramolecular H-transfer within the alkylidene complex $Zr(MeCp)_2(CH_2)$ as described by

$$Zr(MeCp)_2CH_2 \rightarrow Zr(MeCp)(C_5H_4CH_2)Me \qquad (3)$$

The reaction is highly exothermic and $\Delta E = -86$ kJ/mol is calculated. Equation 3 is thus a possible second step of the decomposition of $Zr(MeCp)_2Me_2$, analogous to that reported for $TiCp^*_2Me_2$.[20]

IV. Discussion

The aim of our work is to investigate and understand the mechanism of α-hydrogen abstraction in cyclopentadienyl dimethyl precursor molecules of Ti, Zr, and Hf complexes, which possibly is the first-step reaction in their unimolecular decomposition. Our study can be helpful then in understanding the decomposition of those complexes and in proposing chemical modifications to enhance their thermal stability, thus increasing their utility as precursors for atomic layer deposition.

The decomposition mechanism of Cp complexes of group 4 metals, especially Ti, has been investigated for a long time.[17,24,25] The $TiCp_2Me_2$ complex is the common Petasis reagent,[11] which decomposes according to eq 1 to afford a titanium alkylidene (Schrock carbene)[13,14] that is used in the olefination of carbonyl compounds. This reaction, eq 1, is also used to prepare alkylidene complexes of V^V, Nb^V, Ta^V, Cr^{VI}, Mo^{VI}, W^{VI}, and Re^{VII}.[13,15] $ZrCp_2Me_2$ with oxygen and water was used in MOCVD of ZrO_2 at 400−550 °C. It is possible that the decomposition reaction we present here participated in this MOCVD process in a way similar to the reaction of carbenes with esters in the olefination reaction.[12]

There are still many open questions concerning the critical point of α-hydrogen abstraction—the TS.[13,20] For the first time, we have used DFT to compute the reactants, TSs, and products of eq 1 for group 4 complexes MCp_2Me_2. We have calculated the energetics of the decomposition reaction, and, as expected, the results differ for Ti, Zr, and Hf complexes. Analyzing their geometrical and electronic structures, we are able to explain the differences in TS energetics and in rates of decomposition. The calculated trends in activation energies are in agreement with experimental findings on the thermal stability of Cp complexes.[5,25,33] The excellent agreement between our computed data for $TiCp_2Me_2$ ($E_a = 114$ kJ/mol, $TS_a = -0.02$ kJ/mol) and those measured for the related compound $TiCp^*_2Me_2$ ($\Delta H = 116$ kJ/mol, $T\Delta S = -0.01$ kJ/mol)[20] may be fortuitous given the systematic inaccuracies of DFT. The decomposition reaction leads to a carbene product of high energy which is likely to be

very reactive. We suggest that the carbene rapidly undergoes subsequent reactions with precursor molecules, ultimately aggregating into a solid residue and releasing considerable energy. Equation 1 is thus the rate-determining initial step. This explanation is in agreement with the experimental analysis of cyclopentadienyl precursor molecules of Ti, Zr, and Hf complexes.[5,25]

We therefore suggest that α-H abstraction and decomposition to a methylene complex is not accessible for $Zr(MeCp)_2Me(OMe)$ because the elimination of CH_3OH is much less favored. Our calculations show an overall endothermicity of 299 kJ/mol for this reaction, and, of course, the TS (not calculated here) would be at an even higher energy. This is a plausible explanation for the better thermal stability of $Zr(MeCp)_2Me(OMe)$ over $Zr(MeCp)_2Me_2$.[5] Precursors can therefore be designed to be more thermally stable by avoiding strong hydrogen donors and acceptors in the same molecule.

Returning to ML_2Me_2, Mulliken population analysis reveals that the reactant has a three-center σ $C(CH_4)-M-C(CH_2)$ HOMO with slight M:*d* character (Figure 4), except in the case of $ZrMe_4$, where for symmetry reasons the highest-lying occupied orbitals are five-center σ $M-C_4$. The reactant LUMO is of predominantly M:*d* character. The frontier orbitals at the TS show mixing between HOMO and LUMO; specifically, there is a shift of electron density from one $C(CH_4)$ to other $C(CH_2)$ via M:*d*. We also see that the total charge density of the metal cation (q[M], Table 3) decreases. In this way, the σ $C(CH_4)-M$ bond is broken and a two-center π $M{=}C(CH_2)$ bond is formed. At the TS, the geometry around $C(CH_2)$ suggests sp^2 hybridization, with no remnant of the broken C−H bond visible in the electron density. The product HOMO exhibits π overlap between M:*d* and C:*p*. It seems that transfer of this electron pair by mixing of HOMO and LUMO is the critical point of the reaction, and the associated energy cost dictates the activation energy. We can see therefore that electron transfer will be facilitated if the LUMO is low in energy and the M:*d* orbitals are accessible.

The electrophilicity of M and the ionic character of the M−C bond are known to increase down group 4. Our computed charges on M in the complex agree with this trend (Table 3). The calculated HOMO−LUMO energy gaps also increase down the group and, despite the systematic error in DFT energy gaps, they are a quantitative measure of hardness[34] and, indirectly, of electrophilicity. Of the group 4 metals, the Ti complex has the most *d* character in the HOMO and the lowest-lying LUMO, so for this complex we see the lowest activation energy and predict the most facile decomposition. On the basis of the computed differences in E_a, the Ti complex should decompose 10^5 times faster than the Zr complex at 298 K. Although the ground-state properties of most Zr and Hf compounds are nearly identical,[26] the excited states of the reactant play a decisive role in this reaction, so the higher-lying LUMO of the Hf complex leads to a higher activation energy. Thus, the Hf complex should decompose 10^3 times more slowly than the Zr complex at 298 K. We thus provide evidence for Schrock's suggestion that activation energy increases with the electrophilicity of the metal.[13]

The identity of the ligands can also affect the electrophilicity of the metal, which opens up the possibility of tuning precursor stability via the electronic properties of the ligands. Our calculations show that, relative to L = Cp, alkoxide ligands L = OMe raise the energy of the M:*d*-dominated LUMO, increase the polar character of the M−L bond, and increase the effective charge on M (Table 6). Our computed increase in activation energy correlates with this increase in electrophilicity of the metal. These ligands, although they do not gain/lose atoms in the reaction, are not inert spectators.

The symmetry of the molecule also has an impact on the HOMO−LUMO band gap and consequently on the activation energy of the reaction. The $ZrMe_4$ reactant is of tetrahedral symmetry, and its HOMO is stabilized by delocalization over four M−C bonds (Table 6). This lower-lying HOMO for L = Me means an increase in the energy gap relative to L = Cp, increased hardness, and increased activation energy. Despite this, the symmetry of the complex opens up more degenerate unimolecular and bimolecular channels for H transfer and CH_4 elimination, and MMe_4 complexes are known to be highly unstable.[17]

Analysis of the geometry and the electronic structure suggests that substantial transfer of α-H from $C(CH_2)$ to $C(CH_4)$ has already occurred at the TS, consistent with activation of the C−H bond. Although it may be proposed that this is a Brønsted acid−base reaction (namely, $2(-CH_3^-) \rightarrow {=}CH_2^{2-} + CH_4$ by transfer of H^+), we find no evidence in our calculations for changes in the charge on H as it is transferred from reactant to TS to products. We do see evidence for the transfer of the highest-lying electron pair (HOMO) toward π $M{=}C(CH_2)$ bond, along with the transfer of α-H, as presented in Figure 5. We expect that there is further electron transfer in the cyclic transition state associated with the breaking and formation of C−H bonds, although this is not visible in high-lying orbitals.

Schrock has suggested that α-H is drawn toward a "semi-bridging" position between the reacting ligands.[13] This raises the issue of steric effects on the decomposition reaction. The fact that ligands are more crowded around the smaller Ti center than in the case of Zr and Hf may increase the probability of α-H moving to the semibridging position. Indeed, our data show the Me−M−Me angle closing to a consistent 131−133° at the TS, which involves less distortion of the reactant in the Ti case than in the cases of Zr and Hf (Table 2). For the same reason, the large Cp ligands have an important steric effect in achieving the TS geometry and promoting unimolecular α-H transfer, rather than the bimolecular reaction that predominates for small ligands such as L = Me (Table 5).[17] We have briefly tested the possible TS of the bimolecular reaction described in Scheme 1, eq 2 of ref 17 for $ZrCp_2Me_2$ but have not been able to find such a TS. Even in the case that a bimolecular TS exists, the

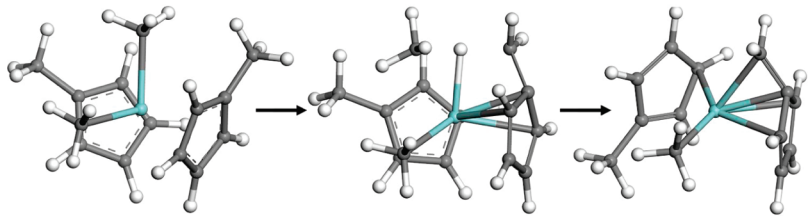

Figure 7. Ball and stick representations of computed structures of precursor (reactant), TS, and product along the decomposition pathway (eq 2) for L = MeCp, M = Zr: white = hydrogen; gray = carbon; blue = Zr.

steric effect of the Cp ligands will encourage unimolecular decomposition over bimolecular.

In the TS, the distance between M and the transferring α-H is short (1.8−2.0 Å) but we find no evidence for electron density between M and H. This can therefore be described as an α-agostic geometry (as opposed to an "agostic bond"), which is a common feature of α-C−H activation by early transition metals.[35] It is thought that the close M−H approach facilitates the breaking or making of M−C bonds.

Our calculations show that Cp ligands play an important role in stabilizing the TS but an even greater role in stabilizing the product (Table 4, Figure 6). The elimination of a methyl group as CH_4 empties a coordination seat on the metal center and destabilizes it. Bulky L = Cp ligands are able to partially cover this seat, while smaller spectator ligands L = Me are not. Furthermore, Cp ligands, due to their partial covalent bonds, M−Cp, decrease the electrophilicity of the metal cation (q[Zr] in Table 6).

Substituents on the Cp ring can open up the possibility of β-hydrogen abstraction. In a case of $Zr(MeCp)_2Me_2$ we have found a TS for transfer of β-hydrogen to give a "tuck-in" complex (eq 2, Figure 7) that has an activation energy similar to that of α-hydrogen abstraction. A complete study of the geometric factors affecting this reaction is beyond the current scope, but it is clear that in such complexes there is competition between abstraction of hydrogens at α and β positions. The situation is complicated by the possibility that the highly reactive carbene (the product of α-hydrogen abstraction, eq 1) may react intramolecularly with substituents on the Cp ring (e.g., eq 3). Contrasting L = MeCp with L = Cp, however, these reactions (eq 2 and eq 3) are not possible for $ZrCp_2Me_2$, which may be the primary difference in the decomposition process of those molecules.

V. Conclusion

The thermal stabilities of the complexes of $M(RCp)_2Me_2$ (R = H and Me) increase down the group of M = Ti, Zr, and Hf. We have used density functional theory to probe a likely decomposition route (α-H abstraction) and characterize the reaction pathway. We find that the activation energy of this reaction increases with the HOMO−LUMO band gap of the reactants, which itself increases with the electrophilicity of the metal cation. The electrophilicity of the metal cation increases down group 4 and can be also influenced by spectator ligands. Examining HOMO and LUMO energies of the reactants ZrL_2Me_2 (L = Cp, OMe, Me) reveals a variety of causes for differences in electrophilicity of Zr and consequently the greater band gap when Cp is replaced by OMe and Me.

The steric effect of the Cp ligands is also visible. The bulky Cp ligands prevent a bimolecular reaction and promote the unimolecular decomposition pathway, as well stabilizing the TS and the product by covering empty coordination seats. In the case of substituted Cp ligands, there may be competition with intramolecular β-H abstraction.

Our model of the decomposition pathway can be used to account for the thermal stability of molecules which undergo this reaction, such as catalysts for olefination reactions. These molecules are also used as ALD precursors, and here the model is helpful in proposing chemical modifications to enhance thermal stability, illustrating how the ALD process window can be widened by rational molecular design based on mechanistic understanding.

Acknowledgment. We gratefully acknowledge the European Commission's Sixth Framework project REALISE (Grant NMP4-CT-2006-016172) for financial support, and we thank S. Rushworth, P. Heys (SAFC Hitech Limited), and M. Leskelä (University of Helsinki) for fruitful discussion.

Note Added after ASAP Publication. This article posted ASAP on January 7, 2010. Minor revisions have been in paragraph 2 of the Introduction section and Table 2. The correct version posted on January 28, 2010.

References and Notes

(1) Wilk, G. D.; Wallace, R. M.; Anthony, J. M. *J. Appl. Phys.* **2001**, *89*, 5243–5275.
(2) Suntola, T. *Mater. Sci. Rep.* **1989**, *4*, 261–312.
(3) Hausmann, D. M.; Kim, E.; Becker, J.; Gordon, R. G. *Chem. Mater.* **2002**, *14*, 4350–4358.
(4) Niinistö, J.; Putkonen, M.; Niinistö, L.; Kukli, K.; Ritala, M.; Leskela, M. *J. Appl. Phys.* **2004**, *95*, 84–91.
(5) Rushworth, S.; Coward, K.; Davies, H.; Heys, P.; Leese, T.; Kempster, L.; Odedra, R.; Song, F.; Williams, P. *Surf. Coat. Technol.* **2007**, *201*, 9060–9065.
(6) Elam, J. W.; Pellin, M. J.; Elliott, S. D.; Zydor, A.; Faia, M. C.; Hupp, J. T. *Appl. Phys. Lett.* **2007**, *91*, 253123.
(7) Puurunen, R. L. *J. Appl. Phys.* **2005**, *97*, 121301.
(8) Elliott, S. D.; Greer, J. C. *J. Mater. Chem.* **2004**, *14*, 3246–3250.
(9) Ziegler, K. H., E.; Breil, H.; Martin, H. *Angew. Chem.* **1955**, *67*, 541–547.
(10) Tebbe, F. N.; Parshall, G. W.; Reddy, G. S. *J. Am. Chem. Soc.* **1978**, *100*, 3611–3613.
(11) Petasis, N. A.; Bzowej, E. I. *J. Am. Chem. Soc.* **1990**, *112*, 6392–6394.
(12) Hughes, D. L.; Payack, J. F.; Cai, D.; Verhoeven, T. R.; Reider, P. J. *Organometallics* **1996**, *15*, 663–667.
(13) Schrock, R. R. *Acc. Chem. Res.* **1979**, *12*, 98–104.
(14) Schrock, R. R. *Chem. Rev.* **2002**, *102*, 145–180.
(15) de Frémont, P.; Marion, N.; Nolan, S. P. *Coord. Chem. Rev.* **2009**, *253*, 862–892.
(16) Davidson, P. J.; Lappert, M. F.; Pearce, R. *Chem. Rev.* **1976**, *76*, 219–242.
(17) Wu, Y.-D.; Peng, Z.-H.; Chan, K. W. K.; Liu, X.; Tuinman, A. A.; Xue, Z. *Organometallics* **1999**, *18*, 2081–2090.
(18) Schrock, R. R. *J. Organomet. Chem.* **1986**, *300*, 249–262.
(19) Alt, H. G.; Di Sanzo, F. P.; Rausch, M. D.; Uden, P. C. *J. Organomet. Chem.* **1976**, *107*, 257–263.
(20) McDade, C.; Green, J. C.; Bercaw, J. E. *Organometallics* **1982**, *1*, 1629–1634.
(21) Bulls, A. R.; Schaefer, W. P.; Serfas, M.; Bercaw, J. E. *Organometallics* **1987**, *6*, 1219–1226.
(22) Schrock, R. R.; Parshall, G. W. *Chem. Rev.* **1976**, *76*, 243–268.
(23) Davidson, P. J.; Lappert, M. F.; Pearce, R. *J. Organomet. Chem.* **1973**, *57*, 269–277.
(24) Beckhaus, R.; Santamaría, C. *J. Organomet. Chem.* **2001**, *617−618*, 81–97.
(25) Mar'in, V. P.; Vyshinskaya, L. I.; Razuvaev, G. A. *Russ. Chem. Rev.* **1989**, *58*, 494–506.
(26) Zheng, W.; Bowen, K. H.; Li, J.; Dabkowska, I.; Gutowski, M. *J. Phys. Chem. A* **2005**, *109*, 11521–11525.
(27) Ahlrichs, R.; Bar, M.; Haser, M.; Horn, H.; Kolmel, C. *Chem. Phys. Lett.* **1989**, *162*, 165–169.
(28) Eichkorn, K.; Treutler, O.; öhm, H.; Häser, M.; Ahlrichs, R. *Chem. Phys. Lett.* **1995**, *242*, 652–660.
(29) Eichkorn, K.; Weigend, F.; Treutler, O.; Ahlrichs, R. *Theor. Chim. Acta* **1997**, *97*, 119–124.
(30) Sierka, M.; Hogekamp, A.; Ahlrichs, R. *J. Chem. Phys.* **2003**, *118*, 9136–9148.
(31) Schafer, A.; Horn, H.; Ahlrichs, R. *J. Chem. Phys.* **1992**, *97*, 2571–2577.
(32) Andrae, D.; Häuβermann, U.; Dolg, M.; Stoll, H.; Preuss, H. *Theor. Chim. Acta* **1990**, *77*, 123–141.
(33) Piper, T. S.; Wilkinson, G. J. *Inorg. Nucl. Chem.* **1956**, *3*, 104−124.
(34) Chattaraj, P. K.; Sarkar, U.; Roy, D. R. *Chem. Rev.* **2006**, *106*, 2065–2091.
(35) Berkaine, N.; Reinhardt, P.; Alikhani, M. E. *Chem. Phys.* **2008**, *343*, 241–249.

JP9072608